Author Manuscript

Title: Origin of Selectivity of a Triazinyl Ligand for Americium(III) over Neodymium(III)

Authors: Thomas Edward Albrecht-Schmitt; David Dan; Cristian Celis-Barros; Frankie White; Joseph Sperling

To be cited as: 10.1002/chem.201806070

Link to VoR: https://doi.org/10.1002/chem.201806070

Origin of Selectivity of a Triazinyl Ligand for Americium(III) over Neodymium(III)

David Dan, Cristian Celis-Barros, Frankie D. White, Joseph M. Sperling, and Thomas E. Albrecht-Schmitt *

Abstract: $[M(EtBTP)_3][BPh_4]_3 \cdot 3CH_3CN$ (M = Nd, Am; EtBTP = 2,6-bis(5,6-diethyl-1,2,4-triazin-3-yl)pyridine) have been synthesized from a reaction of $MCl_3 \cdot nH_2O$ with EtBTP in acetonitrile followed by anion metathesis. Structural analysis reveals that these compounds contain M^{3+} cations bound by tridentate EtBTP ligands to create a tricapped trigonal prismatic geometry around the metal centers. Collection of high-resolution, single crystal X-ray diffraction data also allowed for reduction in bond distance esd's such that a slight contraction of Δ = 0.0158(18) Å in the Am–N versus Nd–N bond distances is observed even though these cations ostensibly have matching ionic radii. Theoretical evaluation revealed enhanced metal-ligand bonding through back donation in the $[Am(EtBTP)_3]^{3+}$ complex that is absent in $[Nd(EtBTP)_3]^{3+}$.

The importance of separating Am^{III} from Ln^{III} (Ln = lanthanide) cations stems from the need for more sensible and efficient nuclear fuel cycles. The recycling of used nuclear fuel centers on the extraction of reusable uranium and plutonium through PUREX-like processes, and their re-use as mixed-oxide (MOX) nuclear fuels.[1] However, storing the remaining waste after this extraction is non-trivial because it is composed of fission products such as ^{90}Sr, ^{137}Cs, and lanthanides, as well as the so-called minor actinides, neptunium, americium, and curium; the latter actinides forming via neutron capture. After extraction of uranium and plutonium, the bulk of the waste consists of either stable isotopes or ones with relatively short half-lives, with notable long-lived exceptions that include ^{99}Tc ($t_{½}$ = 2.11 × 10^5 y) and ^{135}Cs ($t_{½}$ = 2.3 × 10^6 y).

In contrast, americium is mostly present in the form of ^{241}Am, which possesses an intermediate half-life of 432.2 y. Neutron capture and β decay processes primarily from the parent isotope ^{241}Pu create >1.3 kg of americium per ton of typical used nuclear fuel.[2] Thus, the term "minor actinide" is inappropriate for americium and probably needs to be discarded in its entirety. Arguments can be made that it represents an energy resource for fast neutron reactors where it can be fissioned, and that its removal from nuclear waste dramatically decreases the long-term radioactivity of a repository. However, the primary driving force justifying its extraction is the heat load that it creates in nuclear repository scenarios. Accordingly, separating americium from post-PUREX nuclear waste streams has become a focal point of radiochemical interest.

Nitrogen-donor ligands, in contrast to traditional oxygen donors, such as phosphonates and organophosphates, have been the subject of increased attention over the past several decades because of their potential use in *f*-block separations. These complexes possess the added benefit of incineration leading solely to the formation of actinide oxides; thereby reducing the volume of radioactive waste in repositories. One particularly promising family of ligands that falls into this class are the tridentate, nitrogen-rich chelators, based on the bis-triazinyl pyridine (BTP) platform.[3–6] Certain BTP derivatives can be used to achieve high separation factors of >100 for Am^{III} over Eu^{III}.[3–5]

[a] D. Dan, Dr. C. Celis-Barros, Dr. F. D. White, J. M. Sperling, Prof. Dr. T. E. Albrecht-Schmitt
Department of Chemistry and Biochemistry
Florida State University
Tallahasse, Florida 32306 USA
E-mail: albrecht-schmitt@chem.fsu.edu

The separation of americium from both other actinides as well as lanthanides was achieved by the late 1940's using column chromatography and selective precipitation.[7] However, resin-based methods seldom scale well to the large levels needed in the industrial recycling of used nuclear fuel where liquid-liquid extraction has traditionally been preferred. At a fundamental level, if one is to design selective chelators for Am^{III} to be used in biphasic extraction, the first step is to understand its coordination chemistry, which until a decade ago was poorly established.[8–11] The large ionic radius of 1.108(4) Å for eight-coordinate Am^{III},[8] and the availability of a large number of frontier orbitals (5*f*, 6*p*, 6*d*, 7*s*, and 7*p*) that could potentially be involved in bonding gives rise to rich coordination chemistry with americium. Careful design of ligands that target either the cation size or even specific geometries around the metal centers has led to the development of potentially viable complexants for Ln/Am, Am/Cm, and Ln/Cm separations.[12–15]

In this regard, it has been noted that π-back bonding occurs between a singly occupied 5*f* orbital from Am^{III} and a pyridyl nitrogen atom in *N*-2-pyridylmethyl-diethylenetriamine-*N*,*N*′,*N*″,*N*″-tetraacetic acid (DTTA-PyM) that is absent in lanthanide complexes.[16] These studies augment recent work by Adam *et al.* that made use of a ^{15}N-labeled BTP derivative to probe the solution complexation of Am^{III}.[17] Considerably larger ^{15}N NMR shifts were noted in the americium complex than with the corresponding lanthanides. It was inferred that this arose from a greater degree of entanglement of the Am^{III} valence orbitals with ligand-based orbitals in the Am^{III}-BTP complex. However, a solid-state structure of an Am^{III}-BTP complex has yet to be reported. Thus, in this work we provide this information as well as a theoretical framework for understanding the interaction between Am^{III} and a BTP derivative.

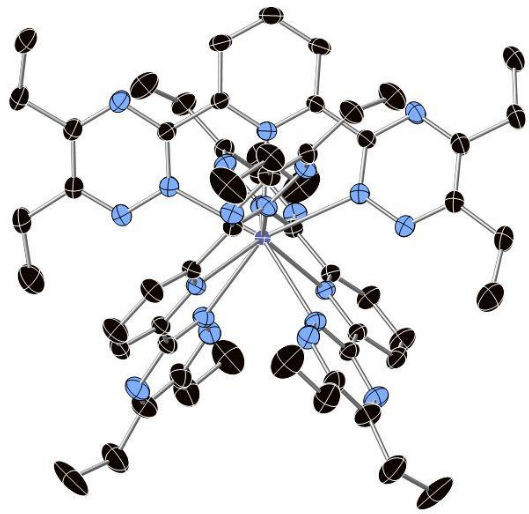

Figure 1. A view of the $[Am(EtBTP)_3]^{3+}$ cation in $[Am(EtBTP)_3][BPh_4]_3 \cdot 3CH_3CN$ with 50% percent probability ellipsoids with hydrogen atoms omitted for clarity.

Nd^{III} is often used as a structural analog of Am^{III} because of their overlapping ionic radii.[8] Thus, it is not surprising that $[Nd(EtBTP)_3][BPh_4]_3 \cdot 3CH_3CN$ and $[Am(EtBTP)_3][BPh_4]_3 \cdot 3CH_3CN$ are isomorphous. These compounds crystallize with unusually high symmetry for molecular systems and are found to adopt tetragonal symmetry in space group $I4_1/a$. Despite a number of rather thorough investigations of $[Am(BTP)_3]^{3+}$ and related complexes,[17–21] a crystal structure has not been reported. We found that the key to growing crystals was to shorten the length of the side chains to just ethyl, and to use $[BPh_4]^-$ as the counter anion for crystallization. This anion would be expected to form intermolecular π-π interactions with EtBTP ligands, and this is observed with the closest contact distance between a EtBTP ligand and an $[BPh_4]^-$ anion at 3.412(4) Å. The co-crystallized acetonitrile solvent molecules aid in filling the voids between these rather large cations and anions.

The $[M(EtBTP)_3]^{3+}$ (M = Nd, Am) complexes are nine-coordinate with distorted tricapped trigonal prismatic geometries and approximate D_3 symmetry, and are thus chiral as expected for any tris-chelate. The centrosymmetric space group indicates that the crystals are a racemic mixture and that spontaneous resolution has not occurred during crystallization. A view of the Δ enantiomer is shown in Figure 1 for the $[Am(EtBTP)_3]^{3+}$ complex. The binding by the EtBTP ligand to the M^{3+} centers occurs through one pyridine moiety and one nitrogen atom from each of the azinyl pendant groups. The Nd–N(pyr) and Am–N(pyr) bond distances are 2.5712(13) and 2.5569(18) Å, respectively. Whereas the Nd–N(azi) and Am–N(azi) bond distances are 2.5751(13) and 2.5648(17) Å, respectively. The average Nd–N and Am–N bond distances are 2.5776(13) and 2.5618(18) Å, yielding Δ = 0.0158(18) Å, which was previously not detected in EXAFS data obtained from these complexes in solution.[22,23] Thus, if one assumes that the ionic radii of Nd^{III} and Am^{III} actually overlap, then additional factors are contributing to contracting the Am–N bonds. Similar observations have been in other N-donor systems with Nd^{III} and Am^{III} as well as in chalcogen-based ligands systems when trivalent lanthanide and actinides are compared.[24,25] We will show that the contraction of the Am–N bonds is the result of back bonding between 5*f* orbitals the EtBTP ligands similar to that observed in the Am^{III} DTTA-PyM complex.[16]

Table 1. Assignment of main *f-f* transitions according to SO-CASSCF wave functions (in nm).

$[Nd(EtBTP)_3]^{3+}$		$[Am(EtBTP)_3]^{3+}$	
Transition	Wavelength	Transition	Wavelength
$^4I_0 \rightarrow {}^4F_{3/2}$	870	$^7F_0 \rightarrow {}^7F_4$	1030
$^4I_0 \rightarrow {}^4F_{5/2}$	800	$^7F_0 \rightarrow {}^7F_6$	810
$^4I_0 \rightarrow {}^2H_{9/2}$	740	$^7F_0 \rightarrow {}^5D_2+{}^5L_6$	525
$^4I_0 \rightarrow {}^2G_{7/2} + {}^4G_{5/2}$	580		
$^4I_0 \rightarrow {}^2K_{15/2}$	520		

The solid-state absorption spectra of both compounds reveal a broad band that spans from ~350 nm to 475 nm as shown in Figure 2. The λ_{max} for this broad peak occurs at 400 nm for both $[Nd(EtBTP)_3][BPh_4]_3\cdot3CH_3CN$ and $[Am(EtBTP)_3][BPh_4]_3\cdot3CH_3CN$. This feature is consistent with a Laporte-allowed, charge-transfer band as well as intra-ligand transitions of the EtBTP ligand. In the case of $[Nd(EtBTP)_3][BPh_4]_3\cdot3CH_3CN$ this broad band is followed by the *f-f* Nd^{3+} transitions.[26] The characteristic $^7F_0 \rightarrow {}^5L_6$ transition of $Am^{3+}_{(aq)}$ at 503 nm is shifted in the solid-state spectra of $[Am(EtBTP)_3][BPh_4]_3\cdot3CH_3CN$ to 524 nm.[27]

Calculated TD-DFT absorption spectra for $[Nd(EtBTP)_3]^{3+}$ and $[Am(EtBTP)_3]^{3+}$ show strong similarities with respect to the experimental results provided in Figure 3. However, the *f-f* transition region is not predicted well by TD-DFT, which is expected if these transitions involve a change in the multiplicity. Furthermore, the broad band in the 300-500 nm range was slightly adjusted for a better fit in the Nd analog (~40 nm) with respect to the experimental data. Table S1 shows the primary transitions involved in the absorption spectra. The nature of the orbitals involved in these transitions are represented in Figure 3, where the mixing is shown in percentages. Orbitals composed purely by ligand orbitals are referred to as π or π* depending on their occupation.

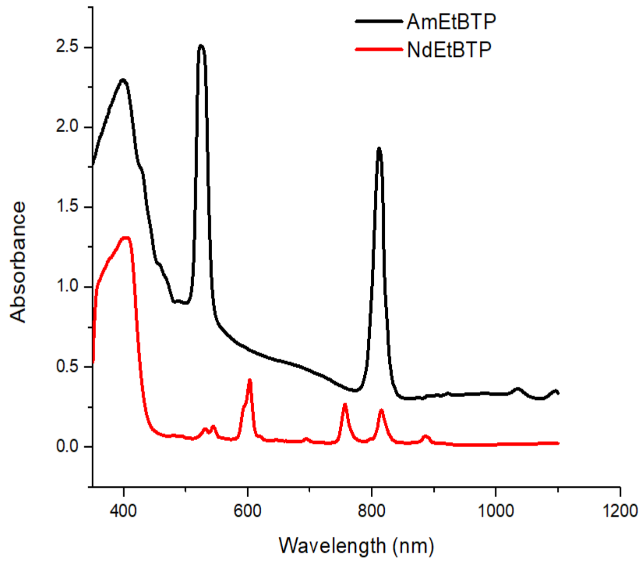

Figure 2. UV-vis-NIR absorption spectra of $[Am(EtBTP)_3][BPh_4]_3\cdot3CH_3CN$ (black) and $[Nd(EtBTP)_3][BPh_4]_3\cdot3CH_3CN$ (red) obtained from single crystals.

According to these TD-DFT results, the *f*-orbitals are not purely metal-based in nature and are mixed with ligand orbitals. Two kinds of mixed orbitals were found in these transitions; orbitals strongly dominated by ligand contributions, and orbitals strongly dominated by the metal, π*f* and σ*f*, respectively (see Figure 4). The broad band can be decomposed into three main transitions according to their oscillator strengths. The first is at ~290-300 nm and shows π→π* and π→π*f* for both complexes. Even though these transitions belong to the same type in the Nd^{III} and Am^{III} complexes, the participation of the *f*-subshell in the Nd^{III} complex is negligible. Moving toward the visible region (350-400 nm), one can observe the main difference between these two complexes. $[Am(EtBTP)_3]^{3+}$ shows transitions attributable to back donation, whereas $[Nd(EtBTP)_3]^{3+}$ only has those attributable to π→π*f*.[28,29] It is clear from these results that $[Am(EtBTP)_3]^{3+}$ displays a different electronic structure than $[Nd(EtBTP)_3]^{3+}$ based on the involvement of the *f*-subshell. The inability of TD-DFT to reproduce *f-f* transitions is addressed by SO-CAS, where the low-lying states are provided in Table S2. Likewise, *f-f* transitions involved in the experimental absorption spectra were assigned through the SO-CAS wave function (Table 1) and agree with those reported elsewhere.[30–33]

Moreover, the nature of the ground states is also different for both complexes. $[Nd(EtBTP)_3]^{3+}$ possesses a multiconfigurational quartet ground state, while $[Am(EtBTP)_3]^{3+}$ has a multireference ground state that is 78% septet and 18% quintet. This is not unexpected because actinides are subjected to stronger spin-orbit coupling than lanthanides, where SOC constants (ζ) are 765.3 and 2656.3 cm^{-1} for $[Nd(EtBTP)_3]^{3+}$ and $[Am(EtBTP)_3]^{3+}$, respectively.

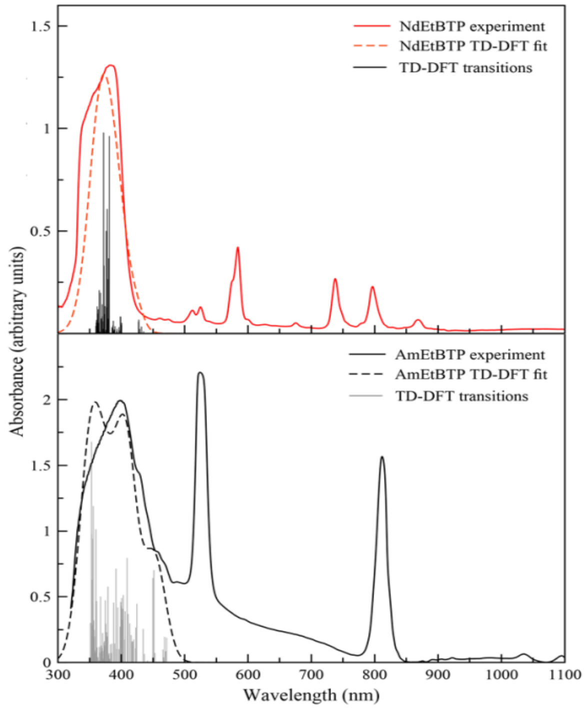

Figure 3. Calculated TD-DFT absorption spectra for $[Nd(EtBTP)_3]^{3+}$ (red dashed line) and $[Am(EtBTP)_3]^{3+}$ (black dashed line). Dashed lines represent a gaussian fitting of the TD-DFT transitions (vertical lines). Experimental data is presented in solid lines.

Ab-initio Ligand Field Theory (AILFT) analysis was also employed to understand how the one-electron F^k interelectronic Slater-Condon parameters are shifted from the free-ion upon complexation.[34] Table 2 contains values for F^2, F^4, F^6 and ζ for free and complexed Nd^{III} and Am^{III} ions. Any reduction in the F^k parameters are indicative of a relaxation of the electron repulsion by increasing correlation between the ligand and the metal that can be seen as an increase in covalency. According to Jung and coworkers,[34] decrements with respect to the free ion larger than 6% are considered as meaningful covalent bonds. In this case, neither $[Nd(EtBTP)_3]^{3+}$ nor $[Am(EtBTP)_3]^{3+}$ present such a significant reduction. However, the latter displays twice the reduction of the former, which is consistent with our TD-DFT calculations supporting back donation in $[Am(EtBTP)_3]^{3+}$. This is in line with the fact that back donation interactions are usually weaker than forward donation, and both are able to reduce the repulsive interaction between electrons.

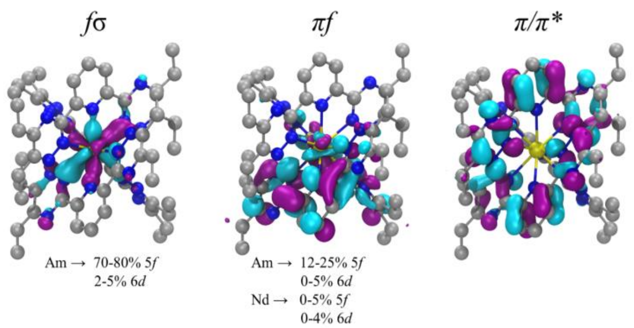

Figure 4. Types of orbitals involved in the absorption spectral features of the $[Nd(EtBTP)_3]^{3+}$ and $[Am(EtBTP)_3]^{3+}$ complexes.

Table 2. Slater-Condon parameters (F^k) and spin-orbit coupling constants derived from Ab-initio ligand field analysis. All values are given in cm^{-1}.

	F^2	F^4	F^6	ζ
Nd^{3+} free ion	99793.6	62590.0	45016.2	772.8
$[Nd(EtBTP)_3]^{3+}$	98366.9	61657.3	44450.2	765.3
Reduction	1.4%	1.5%	1.3%	1.0%
Am^{3+} free ion	82389.8	53831.1	39517.8	2725.9
$[Am(EtBTP)_3]^{3+}$	79973.8	52196.2	38846.1	2656.3
Reduction	2.9%	3.0%	1.7%	2.6%

To obtain a broader picture of bonding in these complexes, topological properties were calculated by means of QTAIM using the SO-CAS wave functions. Table S3 summarizes the main QTAIM parameters where it is possible to note subtle differences in the nature of the electron density localized in the bond critical points (BCPs). The electron densities are similar along all BCPs, but their Laplacian values show considerable differences reflected in H(r) values. These results indicate that despite of the similar electron density accumulation in the BCPs, $[Am(EtBTP)_3]^{3+}$ presents more covalent character than $[Nd(EtBTP)_3]^{3+}$ because of the stronger predominance of the potential energy in those BCPs over Lagrangian kinetic energy. Therefore, the selectivity of EtBTP for Am^{III} over Nd^{III} can be attributed to differences in bonding, and the role of the electrons in the *f*-subshell, where the effects of back donation manifest in the shortened the Am–N bond distances in $[Am(EtBTP)_3]^{3+}$.

In summary, a crystal structure of an $[Am(BTP)_3]^{3+}$ derivative has been obtained through truncation of the BTP side chains and anion metathesis with $[BPh_4]^-$. While this complex and its Nd^{III} analog are isomorphous, the Am^{III} molecule has shorter M–N bond distances than observed with Nd^{III} by 0.0158(18) Å. In both cases the ability to refine datasets to low esd's contributed to the statistical significance of this deviation. This was made possible by the high quality of the crystals and the resultant high mean I/σ, especially at higher than normal diffraction angles. Electronic structure calculations and QTAIM analysis of these complexes supports that the shortened Am–N bonds may be a consequence of back bonding between 5*f* orbitals and the EtBTP ligands as has been observed in other pyridyl ligands.[16,35]

Experimental Section

Caution! Working with ^{243}Am ($t_{1/2}$ = 7370 years) presents potential risks because of its α and γ emission and the emission from its daughter ^{239}Np ($t_{1/2}$ = 2.35 days). All of this work was conducted in a Category II Nuclear Hazard Facility. All manipulations were conducted according to established and approved radiochemical procedures.

Synthesis of 2,6-bis(5,6-diethyl-1,2,4-triazin-3-yl)pyridine. 2,6-bis(5,6-diethyl-1,2,4-triazin-3-yl)pyridine was synthesized by procedure provided in Ref 15. with the only variation being the utilization of 3,4-hexanedione to reduce the length of the alkyl side chains.

Synthesis of $MCl_3{\cdot}nH_2O$ (M = Nd, Am). Multiple 200 μL aliquots of conc. HCl were added to Nd_2O_3 (10.0 mg) or $^{243}AmO_2$ (3.0 mg) and fumed to residues at 150 °C.

Synthesis of $[M(EtBTP)_3][BPh_4]_3{\cdot}3CH_3CN$ (M = Nd, Am). In a 6 mL glass vial, 10.0 mg (27.9 µmol) of $NdCl_3{\cdot}nH_2O$ or 2.5 mg (10.3 µmol) of $AmCl_3{\cdot}nH_2O$ were dissolved in 1 mL of acetonitrile and a few drops of ethanol were added to aid in dissolving the metal salt. This solution was then added to a mixture of 29.2 mg (83.6 µmol) of EtBTP and 50.0 mg of $LiBPh_4$ for Nd or 10.8 mg (30.9 µmol) of EtBTP and 18.4 mg of $LiBPh_4$ for Am dissolved in 2 mL of acetonitrile. The resulting solution was allowed to slowly evaporate overnight yielding large yellow prisms of $[Nd(EtBTP)_3][BPh_4]_3{\cdot}3CH_3CN$ in 77.3 mg (82% yield based on Nd) or reddish-pink prisms for $[Am(EtBTP)_3][BPh_4]_3{\cdot}3CH_3CN$.

Viscous immersion oil was used to adhere single crystals of $[Nd(EtBTP)_3][BPh_4]_3{\cdot}3CH_3CN$ and $[Am(EtBTP)_3][BPh_4]_3{\cdot}3CH_3CN$ to MiTeGen® mounts. They were then optically aligned on a Bruker D8 Quest X-ray diffractometer using a digital camera. Initial intensity measurements were performed using a IµS X-ray source (Mo Kα, λ = 0.71073 Å) with high-brilliance and high-performance focusing multilayered optics. QUEST software was used for determination of the unit cells and data collection control. The intensities of reflections of a hemisphere were collected by a combination of multiple sets of exposures (frames) for $[Nd(EtBTP)_3][BPh_4]_3{\cdot}3CH_3CN$. The standard hemisphere collected on Quest systems limits the resolution to ca. 0.77 Å. The unusually intense diffraction from $[Am(EtBTP)_3][BPh_4]_3{\cdot}3CH_3CN$ facilitated the collection of higher-than-normal resolution diffraction data and the strategy program was used to calculated high-angle shells with high data redundancy.

A Craic Technologies microspectrometer was used to collect the absorption data from single crystals. Single crystals were submerged in immersion oil and placed on a quartz slide in order to collect the optical data. Absorption spectra of $[Nd(EtBTP)_3][BPh_4]_3{\cdot}3CH_3CN$ and $[Am(EtBTP)_3][BPh_4]_3{\cdot}3CH_3CN$ were collected from single crystals of each compound in the EM region from 350 to 1350 nm. Some Am^{III} compounds luminesce when irradiated with short wavelengths. Photoluminescence from $[Am(EtBTP)_3][BPh_4]_3{\cdot}3CH_3CN$ was not observed regardless of excitation wavelength or data collection temperature (down to 79 K),

Computational Details. In order to properly model the electronic structure and properties *f*-block coordination complexes, it is necessary to account for relativistic, ligand, and correlation effects. In order to do so, post-Hartree-Fock methods are recommended in order to account for as much correlation energy as possible. Complete Active Space Self-Consistent Field (CASSCF) calculations have successfully reproduced ground and excited states for f-element complexes as well as capturing ligand-field effects. Scalar relativistic effects are usually considered using the second-order Douglas-Kroll-Hess (DKH2) Hamiltonian and spin-orbit coupling (SOC) by state interaction via QDPT. The ORCA 4.0.1.2 package[36] was used to calculate single- and multi-determinant wave functions. Density Functional Theory (DFT) wave functions were used as starting wave functions to obtain CASSCF wave functions. The Ab-initio Ligand Field Theory (AILFT) module in the ORCA package was used to calculate one-electron Slater-Condon parameters and spin-orbit coupling constants. Am and Nd were modeled using the hybrid PBE0 functional with the SARC-TZVP basis set, while the ligands were modeled using the def2-TZVPP set. Fractional Occupation Density (FOD) analysis[37] was used to determine which orbitals to include in the active space. As expected, the neodymium only required the f-subshell to properly model its properties. In the case of Am, the DFT wave function showed more orbital overlap than expected. Thus, two different active spaces were calculated. The first active space only included the seven 5f orbitals, CAS(6,7) while the second included the seven 5f orbitals plus two ligand orbitals with 5f contribution, CAS(6,9).

Using the resulting spin-orbit corrected wave functions (SO-CAS), Bader's Quantum Theory of Atoms in Molecules (QTAIM)[38] was used to analyze the bonding properties of the Nd^{III} and Am^{III} complexes. Parameters derived from QTAIM were calculated using the MultiWFN program.[39] The most common QTAIM parameters reported are the electron density, ρ(r); the Laplacian of the electron density, $\nabla^2\rho(r)$; the localization, λ(M); and delocalization δ(M-L) indexes. However, $\nabla^2\rho(r)$ values have been proven to always be positive for f-element compounds, whereas purely covalent bonds are characterized by negative $\nabla^2\rho(r)$ values. Instead, energy density parameters give more useful information regarding the nature of the interaction, where if potential energy density, V(r), predominates over the Lagrangian kinetic energy, G(r), the total energy density will be negative and a certain degree of covalency can be attributed to that bond.

Time Dependent DFT (TD-DFT) wave functions were also calculated to identify transitions involved in the absorption spectra. Two functionals were tested, CAM-B3LYP and BP86. Both functionals produced the same absorption spectra with no evidence of f-f transitions. However, these transitions were predicted using the SO-CAS wave function.

Acknowledgments

This research was supported by the Center for Actinide Science and Technology (CAST), an Energy Frontier Research Center (EFRC) funded by the U.S. Department of Energy (DOE), Office of Science, Basic Energy Sciences (BES), under award number DE-SC0016568.

Keywords: Americium complexation •Neodymium complexation • Lanthanide • Actinide • Coordination chemistry

[1] P. D. (Peter D. . Wilson, *The Nuclear Fuel Cycle : From Ore to Wastes*, Oxford University Press, **1996**.

[2] M. Salvatores, G. Palmiotti, *Prog. Part. Nucl. Phys.* **2011**, *66*, 144–166.

[3] Z. Kolarik, U. Müllich, F. Gassner, *Solvent Extr. Ion Exch.* **1999**, *17*, 23–32.

[4] Z. Kolarik, U. Mullich, F. Gassner, *Solvent Extr. Ion Exch.* **1999**, *17*, 1155–1170.

[5] S. Trumm, A. Geist, P. J. Panak, T. Fanghänel, *Solvent Extr. Ion Exch.* **2011**, *29*, 213–229.

[6] Z. Kolarik, **n.d.**, DOI 10.1021/cr078003i.

[7] K. L. Nash, C. Madic, J. N. Mathur, J. Lacquement, in *Chem. Actin. Trans. Elem.*, Springer Netherlands, Dordrecht, **2008**, pp. 2622–2798.

[8] J. N. Cross, E. M. Villa, S. Wang, J. Diwu, M. J. Polinski, T. E. Albrecht-Schmitt, *Inorg. Chem.* **2012**, *51*, 8419–8424.

[9] M. J. Polinski, S. Wang, E. V. Alekseev, W. Depmeier, G. Liu, R. G. Haire, T. E. Albrecht-Schmitt, *Angew. Chemie* **2012**, *124*, 1905–1908.

[10] M. J. Polinski, S. Wang, E. V. Alekseev, W. Depmeier, T. E. Albrecht-Schmitt, *Angew. Chemie* **2011**, *123*, 9053–9056.

[11] J. Diwu, D. J. Grant, S. Wang, L. Gagliardi, T. E. Albrecht-Schmitt, *Inorg. Chem.* **2012**, *51*, 6906–6915.

[12] M. P. Jensen, R. Chiarizia, I. A. Shkrob, J. S. Ulicki, B. D. Spindler, D. J. Murphy, M. Hossain, A. Roca-Sabio, C. Platas-Iglesias, A. de

Blas, et al., *Inorg. Chem.* **2014**, *53*, 6003–6012.
[13] M. P. Jensen, R. Chiarizia, J. S. Ulicki, B. D. Spindler, D. J. Murphy, M. M. Hossain, A. Roca-Sabio, A. de Blas, T. Rodríguez-Blas, *Solvent Extr. Ion Exch.* **2015**, *33*, 329–345.
[14] J. N. Cross, J. A. Macor, J. A. Bertke, M. G. Ferrier, G. S. Girolami, S. A. Kozimor, J. R. Maassen, B. L. Scott, D. K. Shuh, B. W. Stein, et al., *Angew. Chemie* **2016**, *128*, 12947–12951.
[15] G. Modolo, P. Kluxen, A. Geist, *Radiochim. Acta* **2010**, *98*, 193–201.
[16] T. S. Grimes, C. R. Heathman, S. Jansone-Popova, A. S. Ivanov, S. Roy, V. S. Bryantsev, P. R. Zalupski, *Inorg. Chem.* **2018**, *57*, 1373–1385.
[17] C. Adam, P. Kaden, B. B. Beele, U. Müllich, S. Trumm, A. Geist, P. J. Panak, M. A. Denecke, R. Caciuffo, R. Klenze, et al., *Dalt. Trans.* **2013**, *42*, 14068.
[18] A. Bhattacharyya, P. K. Mohapatra, A. Roy, T. Gadly, S. K. Ghosh, V. K. Manchanda, *Hydrometallurgy* **2009**, *99*, 18–24.
[19] Y. WEI, K. N. SABHARWAL, M. KUMAGAI, T. ASAKURA, G. UCHIYAMA, S. FUJINE, *J. Nucl. Sci. Technol.* **2000**, *37*, 1108–1110.
[20] M. Weigl, A. Geist, U. Müllich, K. Gompper, *Solvent Extr. Ion Exch.* **2006**, *24*, 845–860.
[21] A. Geist, C. Hill, G. Modolo, M. R. S. J. Foreman, M. Weigl, K. Gompper, M. J. Hudson, *Solvent Extr. Ion Exch.* **2006**, *24*, 463–483.
[22] M. P. Jensen, A. H. Bond, **2002**, DOI 10.1021/ja0178620.
[23] M. A. Denecke, P. J. Panak, F. Burdet, M. Weigl, A. Geist, R. Klenze, M. Mazzanti, K. Gompper, *BTP) 3. Pour citer cet* **2007**, *10*, DOI 10.1016/j.crci.2006.12.010.
[24] C. Marie, M. Miguirditchian, D. Guillaumont, A. Tosseng, C. Berthon, P. Guilbaud, M. Duvail, J. Bisson, D. Guillaneux, M. Pipelier, et al., *Inorg. Chem.* **2011**, *50*, 6557–6566.
[25] K. I. M. Ingram, M. J. Tassell, A. J. Gaunt, N. Kaltsoyannis, *Inorg. Chem.* **2008**, *47*, 7824–7833.
[26] K. Binnemans, C. Görller-Walrand, *Chem. Phys. Lett.* **1995**, *235*, 163–174.
[27] W. H. Runde, W. W. Schulz, in *Chem. Actin. Trans. Elem.*, Springer Netherlands, Dordrecht, **n.d.**, pp. 1265–1395.
[28] P. B. Iveson, C. Rivière, D. Guillaneux, M. Nierlich, P. Thuéry, M. Ephritikhine, C. Madic, *Chem. Commun* **2001**, 1512–1513.
[29] M. Mazzanti, J. Pécaut, J.-M. Latour, P. Maldivi, M. Remy, **2002**, DOI 10.1021/ic010839v.
[30] J. A. Koningstein, J. E. Geusic, *Phys. Rev.* **1964**, *136*, A711–A716.
[31] B. G. Wybourne, *J. Chem. Phys.* **1960**, *32*, 639–642.
[32] W. T. Carnall, B. G. Wybourne, *J. Chem. Phys.* **1964**, *40*, 3428–3433.
[33] J. N. Cross, E. M. Villa, S. Wang, J. Diwu, M. J. Polinski, T. E. Albrecht-Schmitt, *Inorg. Chem.* **2012**, *51*, 8419–8424.
[34] J. Jung, M. Atanasov, F. Neese, *Inorg. Chem.* **2017**, *56*, 8802–8816.
[35] S. K. Cary, M. Vasiliu, R. E. Baumbach, J. T. Stritzinger, T. D. Green, K. Diefenbach, J. N. Cross, K. L. Knappenberger, G. Liu, M. A. Silver, et al., *Nat. Commun.* **2015**, *6*, 6827.
[36] F. Neese, *Wiley Interdiscip. Rev. Comput. Mol. Sci.* **2012**, *2*, 73–78.
[37] C. A. Bauer, A. Hansen, S. Grimme, *Chem. - A Eur. J.* **2017**, *23*, 6150–6164.
[38] C. F. Matta, R. J. Boyd, *An Introduction to the Quantum Theory of Atoms in Molecules*, **2007**.
[39] T. Lu, F. Chen, *J. Comput. Chem.* **2012**, *33*, 580–592.

Entry for the Table of Contents

COMMUNICATION

Comparison of the Nd^{III} and Am^{III} tris-triazinyl complexes has revealed the nature of the selectivity for Am^{III} over lanthanides.

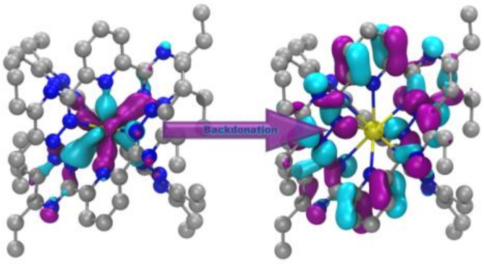

*David Dan, Cristian Celis-barros, Frankie D. White, Joseph M. Sperling, and Thomas E. Albrecht-Schmitt** __________ ***Page – Page***

Origin of Selectivity of a Triazinyl Ligand for Americium(III) over Neodymium(III)